ACS APPLIED MATERIALS & INTERFACES

RESEARCH ARTICLE

www.acsami.org

Superhydrophobic Films on Glass Surface Derived from Trimethylsilanized Silica Gel Nanoparticles

Debmita Goswami, Samar Kumar Medda, and Goutam De*

Nano-Structured Materials Division, Central Glass and Ceramic Research Institute, Council of Scientific and Industrial Research, 196 Raja S. C. Mullick Road, Kolkata 700032, India

Supporting Information

ABSTRACT: The paper deals with the fabrication of sol−gel-derived superhydrophobic films on glass based on the macroscopic silica network with surface modification. The fabricated transparent films were composed of a hybrid $-Si(CH_3)_3$-functionalized SiO_2 nanospheres exhibiting the desired micro/nanostructure, water repellency, and antireflection (AR) property. The wavelength selective AR property can be tuned by controlling the physical thickness of the films. Small-angle X-ray scattering (SAXS) studies revealed the existence of SiO_2 nanoparticles of average size ∼9.4 nm in the sols. TEM studies showed presence of interconnected SiO_2 NPs of ∼10 nm in size. The films were formed with uniformly packed SiO_2 aggregates as observed by FESEM of film surface. FTIR of the films confirmed presence of glasslike Si−O−Si bonding and methyl functionalization. The hydrophobicity of the surface was depended on the thickness of the deposited films. A critical film thickness (>115 nm) was necessary to obtain the air push effect for superhydrophobicity. Trimethylsilyl functionalization of SiO_2 and the surface roughness (rms ≈30 nm as observed by AFM) of the films were also contributed toward the high water contact angle (WCA). The coated glass surface showed WCA value of the droplet as high as 168 ± 3° with 6 μL of water. These superhydrophobic films were found to be stable up to about 230−240 °C as confirmed by TG/DTA studies, and WCA measurements of the films with respect to the heat-treatment temperatures. These high water repellant films can be deposited on relatively large glass surfaces to remove water droplets immediately without any mechanical assistance.

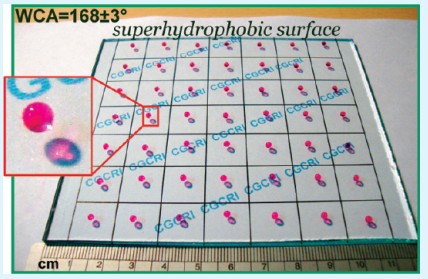

KEYWORDS: trimethylsilanized silica nanoparticles, sol−gel dip-coating, superhydrophobic films, water contact angle, antireflection

1. INTRODUCTION

Inspired by nature, tremendous efforts have been made in replicating its technology. Superhydrophobic surfaces having water contact angle greater than 150° on which water droplets virtually form liquid balls are well-known examples of how design principles adopted from nature can be used in self-cleaning technology. To survive many of the nature's hazards, numerous plant surfaces and body parts of certain insects and animals exhibit superhydrophobic properties.[1−3] The hierarchical structure of the lotus leaf provides one of the classic examples of superhydrophobicity and self-cleaning as studied by Burton and Bhushan[4] and Bhushan and Jung.[5,6] When water droplets sits on the apex of the nanostructures, air bubbles fill in the valleys of the structure underneath it, thus reducing both contact area and adhesion of the droplet to the surface and hence rolls off with a slight tremble. Because of the micronanopatterened structures, these surfaces have attracted a great deal of attention in academia and industry, and thus find wide applications in various fields[7−18] such as in electronic and optical devices,[7] photonic materials,[8] and templates for fabricating biological and chemical sensors.[9] Recently, Song et al. proposed the fabrication of hydrogel and polymeric spheres over a superhydrophobic substrate for potential application in tissue engineering or as support for cell expansion, cell encapsulation and as spherical structures for controlled release of molecule.[19] Wenzel and Cassie theories[20−23] have been widely adopted in correlating the water contact angle (WCA) and surface textures and thus interpreting most of experimental results. A combination of dual scale structure, i.e., surface roughness (micronano combined) and low surface free energy results in artificial superhydrophobic surfaces. Attempts have been made in fabricating and mimicking such surfaces applying coatings with high WCA.[24−36] Because of huge scientific and technological interests several groups have reported fabrication of silica aerogel based superhydrophobic surfaces using the sol−gel techniques.[37−43] Prakash et al.[41] reported the preparation of silica aerogel thin films at ambient pressure without the need of supercritical extraction. The inorganic gel is derivatized with the aid of organosilanes which showed "spring back" effect. The hydrophobic organosilyl terminated surfaces do not participate in condensation reaction, and thus the gel springs back to the porous state. Barkhudarov et al.[42] prepared superhydrophobic films using fluoroalkyl silanes and studied their effectiveness as corrosion inhibitor using neutron reflectivity technique. Budunoglu et al.[28] reported a thermally stable flexible and highly porous aerogel thin films having superhydrophobic properties

Received: May 24, 2011
Accepted: August 8, 2011
Published: August 08, 2011

dx.doi.org/10.1021/am200666m | ACS Appl. Mater. Interfaces 2011, 3, 3440–3447

using a colloidal dispersion of an intrinsically hydrophobic organosilane monomer at ambient conditions. Manca et al.[43] prepared superhydrophobic antireflective coatings using a bilayer approach through the sol−gel process. They used trimethylsilanized silica nanoparticles (Aerosil) partially embedded into an organisilica binder matrix and claimed that the cured (350 °C) coatings have retained the superhydrophobicity even after 2000 h of outdoor exposure. All these reports have incompleteness from several points of view e.g. thermal stability of these superhydrophobic coatings, dependency of coating thickness with WCA, homogeneity with respect to transparency, variation of WCA in reasonably large coated area, development of antireflection properties with tunable transmission maxima, structure of these coatings and so on. In this study, we present a simple, inexpensive sol−gel dip coating procedure which is based on the preparation of a macroscopic network with silica gel nanoparticles (NPs) through the hydrolysis of silicon alkoxide and condensation of silanols. We have achieved to prepare homogeneous trimethylsilanized SiO_2 NP-based films applicable for relatively large area of glass substrates having contact angle 168 ± 3° with transmission up to 95% in desired wavelength without using any flouroalkyl silanes. The detailed characterization of the films considering the above-mentioned points have been made.

2. EXPERIMENTAL SECTION

2.1. Materials. All chemicals were used as received. Tetraethoxy silicate (TEOS) was supplied by Fluka. 1,1,1,3,3,3-hexamethyl disilazane (HMDS) was obtained from Sigma-Aldrich, while n-propanol, methanol (MEOH) and hydrochloric acid (HCl) were received from Ranbaxy fine chemicals, ammonia solution (about 25%, AR) and n-hexane were supplied by s.d. fine-chem limited. Millipore water (resistivity ∼18 MΩ.cm) was used throughout this study.

2.2. Preparation of Trimethyl Silyl [-Si(CH$_3$)$_3$] Modified SiO$_2$ Sol. First SiO_2 sol was prepared at room temperature by hydrolyzing tetraethoxysilane (TEOS) in presence of ammonium hydroxide (NH_4OH) and methanol. In a typical preparation 5 g of TEOS was first dissolved in 8 g of methanol, and to this solution a mixture of 7.5 g of 0.02N NH_4OH and 8 g of methanol was added with stirring. At this stage, pH of this solution was close to 9. The concentration of equivalent SiO_2 in the above mixture was maintained at ∼5 wt %. To the above mixture 3.65 mL of 0.1N HCl was added and kept stirring for another 2 h. The whole solution was turned into gel by adjusting the pH close to 8 by adding requisite amount of NH_4OH solution and kept overnight (16 h) for aging. To prepare methyl-modified SiO_2, 1,1,1,3,3,3-hexamethyl disilazane (HMDS) in n-hexane with 1:8 in wt/wt ratio (molar ratio of HMDS to TEOS were varied at 0.5, 1.0, and 1.5) was added and kept at 60 °C for another 16 h in closed container. Gels so obtained were filtered, washed with n-hexane and subsequently twice with n-propanol, ultrasonicated by adding n-propanol (45 g) for dispersion, and finally centrifuged (1000 rpm/10 min) to obtain the sol for film deposition.

2.3. Preparation of Films. Prior to the film deposition, the float glass substrates (up to a dimension of 115 × 110 mm^2 in size; thickness 2−3 mm) were cleaned by detergents followed by rinsing with water and finally dipping in a hot isopropanol bath. The films were prepared by the dipping technique (Dip-master 200, Chemat Corporation) with a withdrawal velocity of 2−20 cm min^{-1}. The coatings were first dried at 60 °C for 1 h and finally cured at 140 °C for 2 h in an air oven. The thicknesses of the cured (140 °C/2 h) coatings so obtained are varied from ∼90−500 nm depending on the volume of solvent used for the dispersion of trimethylsilanized SiO_2 gels and the withdrawal velocity of the glass substrates from the sols.

2.4. Characterization. The thickness and refractive index (n) of the films deposited on glass substrates were measured by a spectroscopic Ellipsiometer (J. A. Woollam). The UV−visible spectra of the film-coated soda-lime float glass substrates were obtained with a Cary 50 scan spectrophotometer. TG/DTA measurements were done with a Netzsch STA model 409c thermal analyzer using a dynamic heating rate of 3° min^{-1}. Fourier transformed infrared (FTIR) absorption spectra of the films (deposited on intrinsic Si wafers) were recorded using a Nicolet 380 FTIR spectrophotometer with 200 scans for each sample. Small angle X-ray scattering (SAXS) studies of the superhydrophobic sols were done with a Rigaku SmartLab (operating at 9 kW) using Cu Kα (λ = 1.5406 Å) radiation. For this study sols were taken in a sealed silica glass capillary of diameter 1 mm and analyzed. Rigaku NANO solver software was used to estimate the particle size distribution using SAXS data. Field emission scanning electron microscopy (FESEM) analysis was done by Carl Zeiss, Germany, SUPRA-35VP instrument. Atomic force microscopy (AFM) study (contact mode) of the films was made by a Nanonics instrument. Transmission electron microscopy (TEM) measurements were carried out with a Technai G^2-30ST(FEI) operating at 300 kV. TEM samples were prepared by drop casting the diluted final sols onto the carbon-coated Cu grid and then dried at 60° for 1 h followed by curing at 140 °C for 2 h. Contact angle measurements were done with a KRUSS GmbH instrument (easy drop DSA20E model) using 6 μL water droplets in ambient condition. Water contact angle (WCA) value was estimated after averaging 50 measurements in different areas of a 115 × 110 mm^2 coating surface. Thermal stability of the films was evaluated by treating the films at different temperatures.

3. RESULTS AND DISCUSSION

As mentioned in the Experimental Section, wet silica gel was first prepared by a typical sol−gel hydrolysis−polycondensation reaction of tetraethylorthosilicate (TEOS) at pH 9. The reaction can be represented by the following (eq 1)[44]

$$n\mathrm{Si(OC_2H_5)_4} + 2n\mathrm{H_2O} \rightarrow n\mathrm{SiO_2} + 4n\mathrm{C_2H_5OH} \quad (1)$$

The surface of these gels containing numerous numbers of hydrophilic OH groups (∼4−6/nm^2)[45] are reacted with 1,1,1,3,3,3-hexamethyl disilazane (HMDS) to convert a major amount of the OH groups by −OSi(CH$_3$)$_3$ (trimethylsilyl) according to the following reaction (eq 2)[37]

$$2-\mathrm{OH} + (\mathrm{CH_3})_3\mathrm{SiNHSi(CH_3)_3} \rightarrow 2-O-\mathrm{Si(CH_3)_3} + \mathrm{NH_3}\uparrow \quad (2)$$

The above reaction leads to the formation of hydrophobic gels. The washed gels were then sonicated (30 ± 3 kHz, 40−50 min duration) in n-propanol, to form a uniformly dispersed sols of SiO_2 NPs covered with hydrophobic −OSi(CH$_3$)$_3$ groups. This dispersion was used to prepare transparent films on cleaned soda-lime float glass. The SiO_2 NPs covered by the nonhydrolyzable methyl groups prevent the collapsing of pores during solvent evaporation[41,46] and thereby forming a highly porous structure.

We tried to correlate the amount of HMDS used with respect to the equivalent SiO_2 for dehydroxylation and the optical and hydrophobic properties of the resulting films. For this purpose, 3 sols were prepared using 0.5, 1, and 1.5 mols of HMDS with respect to the 1 mol of TEOS. The obtained sols (see Experimental Section) were applied on glass surfaces following a suitable quarter lambda (λ) optical design.[47] It has been observed that the % transmission (in a given λ) of the resulting films decrease continuously with increasing HMDS concentration. The sol prepared with high HMDS concentration (1.5 mol)

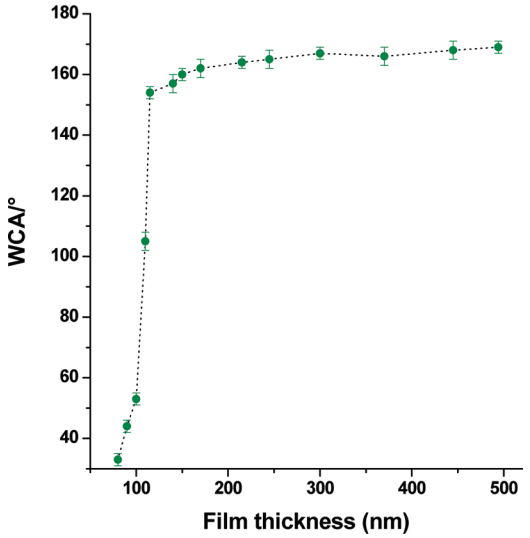

Figure 1. Plot of water contact angle (WCA) values with respect to the film thickness (nm). Films were deposited on float glass substrates and cured at 140 °C for 2 h. Data points are joined for visual guide.

showed a maximum transmission of ~92% (at ~525 nm), whereas the intermediate (1 mol) and low (0.5 mol) HMDS concentrations gave the maximum transmission values ~95 (at ~545 nm) and 96% (at ~555 nm), respectively. Although the transmission of the later case (lowest HMDS) was slightly more, its superhydrophobic property (WCA ~146°) was not good enough as compared to the films obtained from the sols using 1 and 1.5 mol HMDS, where WCA values were 157 and 160°, respectively. So, this result showed that the transparency and superhydrophobicity of the coatings can be controlled by adjusting the HMDS concentration. As the trimethylsilanized silica film is nonabsorbing in the visible wavelength of light with very low refractive index (~1.1) value, it is expected that the porous structure of the films cause scattering of light and eventually control the transmission in the visible region. The use of high amount of HMDS (1.5 mol %) is expected to increase the rate of reaction with an increase in local concentration of ammonia (see eq 2). This may lead to increase the size of the silica aggregates, resulting in more light scattering and hence lower transparency. In cases of 0.5 and 1 mol % HMDS, formation of smaller aggregates is expected because the films show relatively more transmission due to less scattering.[48−50] As the use of 1 mol % HMDS produces good hydrophobicity as well as transparency, detailed characterization and evaluation of these films were made and reported in this work.

The superhydrophobic films deposited on cleaned soda-lime float glass substrates appeared visually clear and spot-free. These films can be applicable for large area surfaces. It has been observed that the hydrophobicity of film surface depends on the thickness of the films.[51,52] The thickness of heat-treated (140 °C/2 h) films and the corresponding measured WCA values are plotted and presented in Figure 1. As shown in the figure that the WCA values are very low (33−53°) when film thickness values are less than 100 nm. The surface has started to become superhydrophobic (WCA >150°) when film thickness value approaches >115 nm. The films showed very high WCA values (160−171°) in the thickness ranges ~150−500 nm. We observed extreme superhydrophobicity in cases of films having thickness values ~300 nm and above. In such cases, WCA values

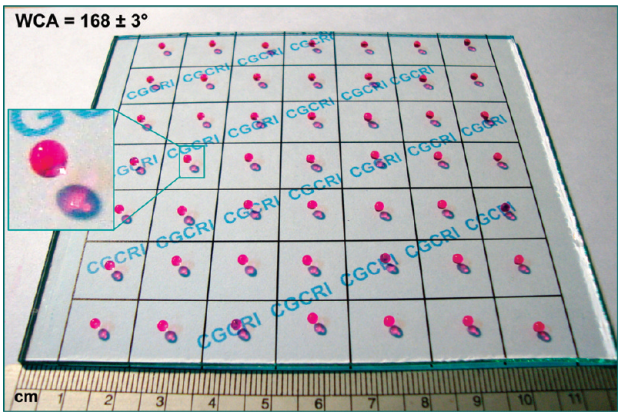

Figure 2. Photograph of water drops on superhydrophobic film coated float glass (size 115 × 110 mm^2). A magnified view of one of the drops is shown in the inset.

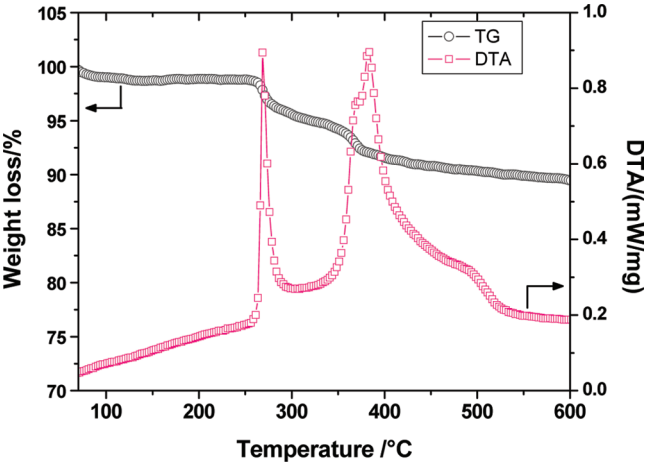

Figure 3. TG/DTA of the superhydrophobic powder sample. Measurement was performed at a heating rate of 3 °C min^{-1} in air.

as high as 171° were observed and it was difficult to place a water drop on the surface.

Four parameters can be accounted for the phenomenon of superhydrophobicity, namely chemical modification of the surface by hydrophobic trimethyl groups, surface roughness (related to the porous structure), thickness of the film and the underlying glass substrate which is relatively hydrophilic in nature. Affixing two of them i.e. surface modification by hydrophobic groups and the surface structure, primarily two counter-acting forces are acted on the water droplet i.e. the up thrust of air (air push) entrapped in the nanogrooves (pores) and the electrostatic attraction force between the water droplet and the hydrophilic glass surface.[53] With increasing coating thickness, concentration of nanogrooves formed by the agglomeration of SiO_2 NPs per unit area will be more resulting in the greater up thrust of air and thus a globular water droplet (high WCA) on the surface is formed. However, when coating thickness decreases, the electrostatic attraction force between the hydrophilic glass surface and water droplet predominates over the air push, and thus water droplet comes in close proximity with the glass substrate, resulting in a flatter water droplet (low WCA). Here we have found a critical film thickness value of ~115 nm and above which is essential to obtain superhydrophobic properties of the surface.

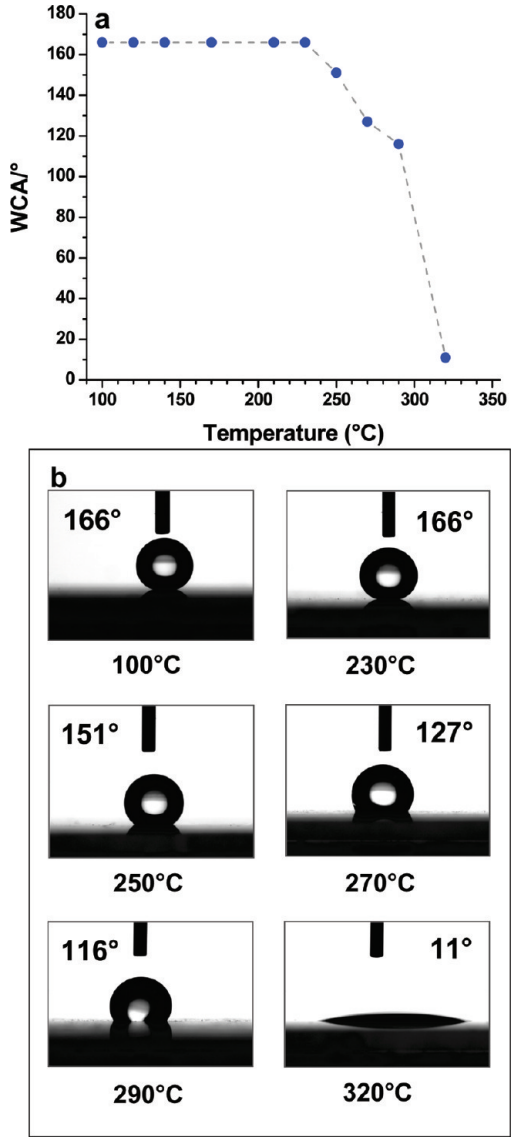

Figure 4. (a) Plot of heat-treatment temperatures of the films vs WCA. The data points are joined by a dashed line for visual guide. (b) Images of water droplets as observed by the contact angle meter during the transformation of superhydrophobic (WCA 166°) to hydrophilic (WCA 11°) surface. As the WCA remains unchanged from 100−230 °C the intermediates are not shown. The film of thickness ∼350 nm was deposited on glass surface and heat-treated in an oven at different temperatures (100−320 °C) in a cumulative heating procedure with a holding time of 2 h in each step. The WCA was measured with 6 μL water droplets in all cases.

Figure 2 shows a representative photo of a 115 × 110 mm^2 float glass coated with superhydrophobic film of thickness ∼400 nm. The water droplets (decorated with red dye) take perfect spherical shape and appeared almost like floating on the surface (see the magnified inset of Figure 2). The average WCA value measured at 50 different places was found to be 168 ± 3° with 6 μL water droplets.

3.1. Thermal Stability of the Films. The final hydrophobic sol was evaporated to dryness and then heat-treated at 140 °C for 2 h, and subjected to thermogravimetry (TG) and differential thermal analysis (DTA) studies. The results are presented in Figure 3. It was observed that the material did not decompose

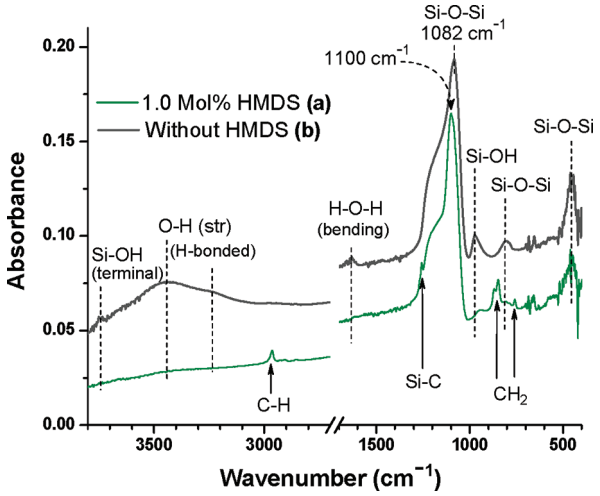

Figure 5. FTIR spectra of the films deposited on both side polished intrinsic Si wafer. (a) Superhydrophobic film of thickness ∼350 nm prepared using HMDS and (b) similar film prepared without using HMDS. Both films were cured at 140 °C/2 h. Absorbance scale has been shifted for clarity.

until about 255 °C. The TG curve showed no noticeable weight loss up to about 255 °C, and after that the decomposition of organic components (mainly methyl groups) was started exothermically. The decomposition took place mainly in two steps as observed from the TG curve; however the corresponding DTA showed a more complex nature of decomposition showing a sharp exothermic peak at 270 °C followed by a relatively broad exothermic peak at 383° flanked by two shoulders at 368 and 492 °C. We have also studied the thermal stability of the films with respect to the WCA. For this purpose films of about 350 nm in thickness (film thickness was checked after curing at 140 °C/2 h) was prepared on glass substrate and WCA values were measured with respect to the thermal treatment temperatures in the range 100−320 °C with a holding time of 2 h at the respective temperatures. The data are presented in Figure 4a. The images of water droplets as observed by the contact angle meter are also shown in the panel b of Figure 4. The films heat-treated up to 230 °C showed no deterioration of the surface and the WCA remained same at 166° (Figure 4a,b). The WCA started to decrease at 250 °C and gradually became hydrophilic showing WCA of only 11° at 320 °C. This observation indicated that the decomposition of organic groups at about 320 °C led to the formation of hydrophilic silanol surface (Figure 4b). The difference of decomposition temperatures in cases of TG/DTA (>255 °C) and oven heating (>230 °C) is due to the different heating conditions. In case of TG/DTA the sample was heated in a dynamic condition (heating rate of 3° min^{-1}) whereas oven heating was performed at fixed temperatures with a holding time of 2 h. So in the latter case, the sample got enough time to decompose at relatively low temperature.

3.2. Structure of Films. The structure of film materials was analyzed by FTIR, SAXS, TEM, FESEM, and AFM techniques.

3.2.1. FTIR Studies. The chemical bonding of the dip-coated superhydrophobic silica films heat-treated at 140 °C for 2 h was investigated by the FTIR spectroscopy. For this purpose films were deposited on intrinsic Si wafers and heat-treated in a similar way as that of films on glass substrates. Films prepared from sol without using HMDS was also studied for comparison. Figure 5

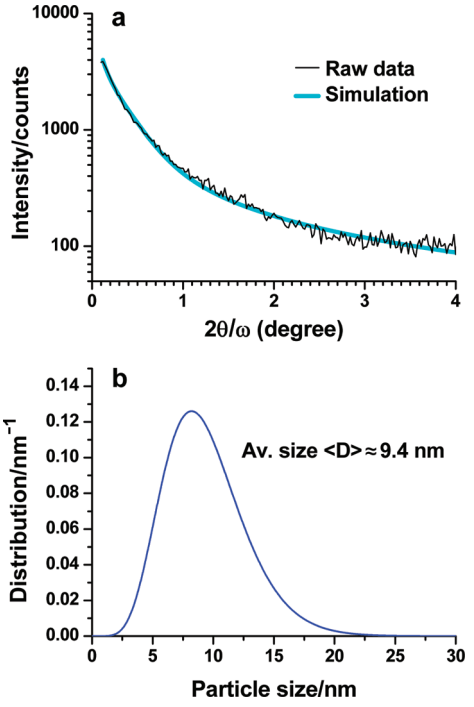

Figure 6. (a) Transmission SAXS profile of the superhydrophobic sol along with the simulated curve using a spherical particle model, and (b) size distributions of the silica nanoparticles estimated from the SAXS profile using the NANO solver software.

shows FTIR spectra of the trimethylsilanized superhydrophobic film of thickness ~350 nm along with HMDS untreated silica gel films. Both the films were cured at 140 °C for 2 h. The silica gel films showed characteristic O−H related peaks at 3742 (terminal/free O−H), 3443 (broad) and 3236 (O−H stretching), 968 (Si−OH) and Si−O−Si originated bands at 1082 (Si−O−Si asymmetric stretching), 810 and 453 cm^{-1} (Si−O−Si symmetric stretching).[43,54] The corresponding trimethylsilanized superhydrophobic film showed almost absence of all the O−H related bands. The spectrum showed presence of several Si−$(CH_3)_3$ group related peaks at 2964, 2906 (C−H stretching), 1258 (Si−C), 879, 848, and 756 cm^{-1} (CH_2 rocking)[43,54,55] and a strong peak at 1100 cm^{-1} due to Si−O−Si asymmetric stretching. The presence of Si−CH_3− peaks and almost disappearance of −OH related bands revealed that most of the Si−OH groups were successfully substituted by the Si−O−Si$(CH_3)_3$ as shown by eq 2. It can be noted here that the Si−O−Si asymmetric stretching (TO mode) of the superhydrophobic film shifted significantly toward higher wavenumber (1100 cm^{-1}) compared to the HMDS untreated silica film (1082 cm^{-1}). The appearance of this band near 1100 cm^{-1} indicated the formation of glasslike silica structure as glassy silica absorbs close to this region due to Si−O−Si.[56]

3.2.2. Small-Angle X-ray Scattering (SAXS). SAXS studies were undertaken to estimate the particle size distributions of the silica clusters in the final sol. It is now established that SAXS analysis can give accurate particle size with its distribution.[57] Figure 6a shows the experimental transmission SAXS profiles obtained from the final hydrophobic silica sol. The simulated curve using a spherical particle model is in good agreement with the measurement (Figure 6a). Figure 6b shows the particle size distribution obtained from such SAXS profile. The average size of the particles was estimated to be 9.4 nm with a dispersion of ~35%.

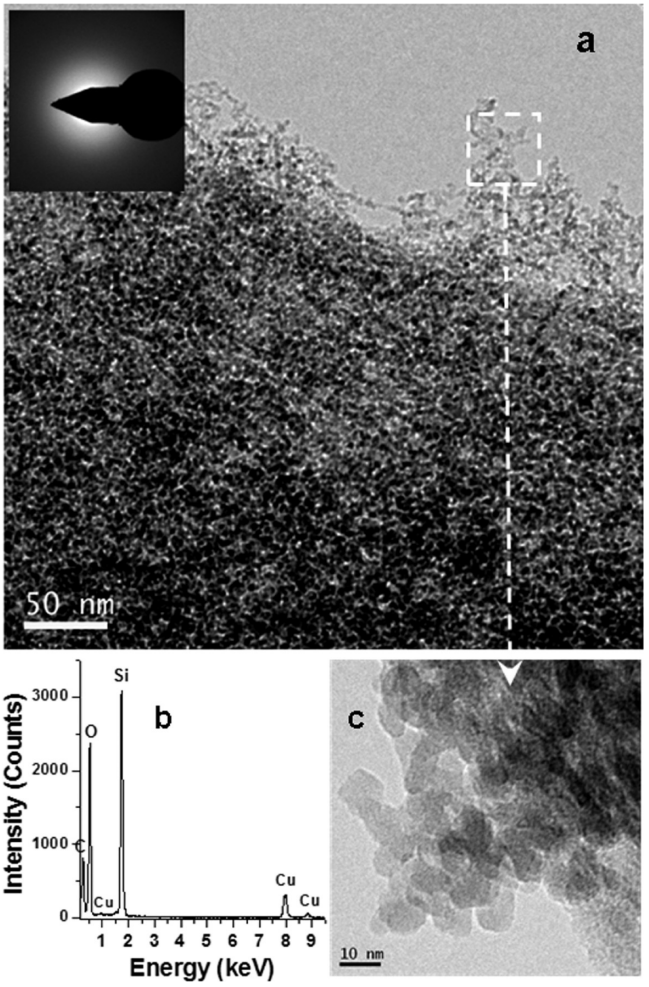

Figure 7. TEM images of the superhydrophobic film material cured at 140 °C/2 h: (a) low-resolution image showing interlinked agglomerated SiO_2 NPs, (b) EDX spectrum, and (c) image of a marked portion of (a) in a magnified resolution. SAED pattern is shown in the inset of (a). Cu peaks appeared in the EDX spectrum are from the Cu-grids used for TEM study.

3.2.3. Transmission Electron Microscopy. The microstructure of the silica clusters in the dispersed sol was examined by TEM. For this purpose diluted hydrophobic sol was drop casted on a carbon coated Cu grid, dried and cured at 140 °C for 2 h prior to TEM study. TEM bright field image presented in Figure 7a shows presence of interlinked SiO_2 clusters of size ~10 nm. The average particle size distribution obtained by SAXS matched very well with the TEM. The EDX analysis (Figure 7b) confirms the presence of Si and O in the material. The Cu peaks observed in the EDX pattern are from the Cu grid used for TEM study. The carbon peak (Figure 7b) is mainly from the carbon coated grid with some contribution from the surface methyl groups of the sample. SAED pattern presented in the inset of Figure 7a confirms the amorphous nature of silica. A representative portion of the low resolution image (marked by square box in Figure 7a) was observed by TEM with high magnification and presented in Figure 7c. Agglomerated silica clusters of about 10 nm in size are clearly visible in this image.

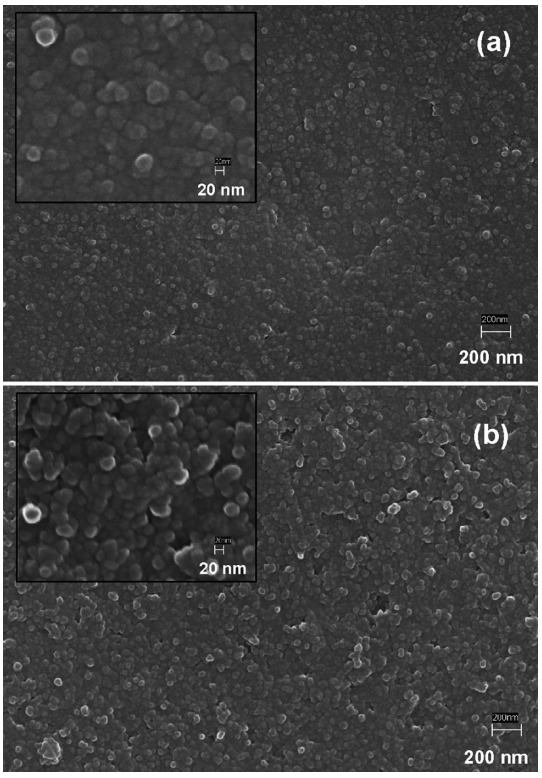

Figure 8. FESEM images of films having thickness (a) ~100 and (b) ~350 nm. The WCA values of low (~100 nm) and high (~350 nm) thickness film surfaces were ~53 and 167°, respectively.

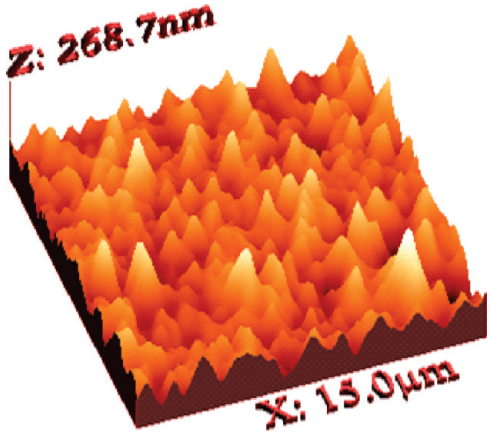

Figure 9. AFM image showing the surface topography of a representative film of thickness ~350 nm. The rms surface roughness value obtained from the image is ~30 nm.

3.2.4. FESEM Study. The film surfaces were observed by the FESEM in order to see the surface microstructure. For this purpose two representative cured (140 °C/2 h) films of thickness ~100 and ~350 nm were analyzed. The low thickness (~100 nm) film was of particular interest to check the presence of any inhomogeneity of the film deposition. FESEM images of the films are shown in Figure 8a,b. Both the (a) low and high (b) thickness films show complete coverage of the substrate[58] with uniformly packed SiO_2 nanoaggregates. The size of the SiO_2 nanoaggregates vary in the range of ~10−30 nm (see the magnified image presented in the respective insets). It is expected that the larger aggregates were formed with the agglomeration of smaller particles (~10 nm) during the formation of such well packed films. Although the glass surface was covered by films in both the cases, it should be noted here that the low and high thickness films showed very different WCA values of ~53° and ~167°, respectively. So thickness of the film has a pronounced effect in controlling the hydrophobicity as discussed before (see Figure 1 and related discussion).

3.2.5. Atomic Force Microscopy. The hydrophobicity of a surface is dependent both on its chemical composition and topography.[59] AFM study of one representative hydrophobic film of thickness ~350 nm was undertaken to see the surface topography. Figure 9 shows AFM image of the film covering an area of 15 × 15 μm^2. The surface of the film was found to be spiky in nature with a root-mean square (rms) roughness value of about 30 nm. This spiky topography favors high hydrophobicity of the film surface.

3.3. Antireflection (AR) Property. The trimethylsilanized SiO_2 sol is composed of many nanosized spherical amorphous SiO_2 nanoparticles (NPs) having an average diameter of ~10 nm. The films are constituted by interlinking of these SiO_2 NPs with each other, and the stacking of these particles constructs void pores inside the film which makes the refractive index of film (n_f) lower than the index of the substrate (n_s), and as a result, the films become antireflective (AR) in nature. The films produced in this work showed a refractive index value of 1.10 ± 0.01 with very low extinction coefficient (k) values. Very low k value throughout the visible range indicates that the film is nonabsorbing in nature. Ellipsometric measurement of one representative film showing refractive index (n) and extinction coefficient (k) values is presented as Supporting Information (Figure S1). On the glass substrates we have deposited such hydrophobic porous coatings of different $\lambda/4$ thickness values, keeping in view obtaining single layer AR films (Table 1). For the deposition of such coatings first a calibration curve of thickness (t) values with respect to different withdrawal velocities (v) of the substrates was made (see Figure S2 and related discussion; Supporting Information). Using this calibration graph v was calculated to obtain the required $\lambda/4$ thickness of films.[47] Figure 10 shows that the position of transmission maxima of the coated glass can be tuned by

Table 1. Optical and Physical Thickness Values of Superhydrophobic Films for Obtaining Maximum Transmission at a Desired Wavelength Considering the Refractive Index (RI) of the Film 1.10 ± 0.01[a]

min reflection or max transmission (nm)	optical thickness ($\lambda/4$) (nm)	physical thickness = optical thickness/RI (nm)	experimentally observed wavelengths (nm)	max % transmission
500 (AR1)	125	113.6	500 ± 20	95.2
550 (AR2)	137.5	125	550 ± 20	95.2
600 (AR3)	150	136.4	600 ± 20	95.2

[a] The calculation was based on the single-layer $\lambda/4$ optical designs for AR effect. Both the desired and observed transmission maxima values are given.

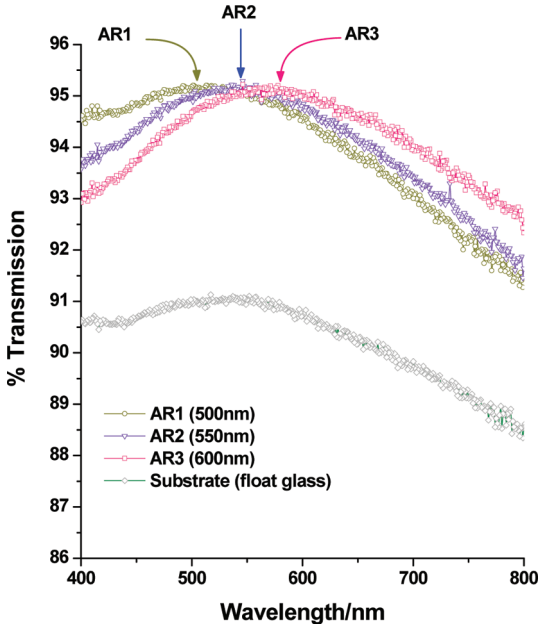

Figure 10. Transmission optical spectra of single-layer AR-coated glass substrates. The position of transmission maxima were tuned by controlling the $\lambda/4$ optical designs. Transmission spectrum of uncoated glass is also shown.

controlling the thickness of hydrophobic film layers after curing. The transmission curves of films deposited using different $\lambda/4$ thickness values corresponding to 500 (AR1), 550 (AR2) and 600 nm (AR3) are shown in the above-mentioned figure. The same sol was used to deposit such set of films. As shown in Figure 10, the experimental curves follow closely to the given optical designs. In cases of AR1, AR2 and AR3 the peak maxima appeared at 503, 545, and 581 nm, respectively.

The % transmission is found to be increased from 91 (uncoated glass) to more than 95 at the predetermined wavelengths (Table 1). In general a refractive index of less than 1.22 is ideal for an AR film having ~100% transmission value. Although the measured RI values of these hydrophobic coatings are less than 1.22 we could achieve a maximum transmission value of little higher than 95%. As the films are nonabsorbing in nature, it is expected that the scattering of light originating from the SiO_2 agglomerates is mainly responsible for the loss of transmission.

4. CONCLUSIONS

The above studies demonstrated synthesis of trimethylsilanized SiO_2 nanosphere based superhydrophobic coatings applicable for large area glass surfaces and their detailed characterizations keeping in view applications. We showed here that the amount of surface modifying agent HMDS in the sol and the coating thickness are two important parameters to obtain high WCA ($168 \pm 3°$) as well as tunable AR effects. The study revealed that a critical thickness is necessary in obtaining the desired air push effect for superhydrophobicity. The thickness of the film, its porosity, surface roughness and $-Si(CH_3)_3$ functionalization, all in combination yielded high-performance superhydrophobic coatings. These coatings can find applications as self-cleaning surfaces with optical benefits (AR effects). The formation of perfect spherical water balls on these large area superhydrophobic substrates can find potential applications in the synthesis of water-soluble highly spherical hydrogels incorporated with cells, antibodies, drugs and related biomaterials.[19] Such surface is useful in protein microarray chip technology.[60] This superhydrophobic substrate can also find applications in medical diagonistics where large numbers of water-soluble specimens in the form of isolated spots (drops) can be analyzed simultaneously.

■ ASSOCIATED CONTENT

Supporting Information. Refractive index and extinction coefficient curves of one representative film sample (Figure S1) and calibration curve of film thickness with respect to the withdrawal velocities for AR coating deposition (Figure S2). This material is available free of charge via the Internet at http://pubs.acs.org.

■ AUTHOR INFORMATION

Corresponding Author

*Tel: +91 33 24733469/96, ext. 3403. Fax: 91-33-24730957. E-mail: gde@cgcri.res.in.

■ ACKNOWLEDGMENT

Council of Scientific and Industrial Research (CSIR), New Delhi, India is thankfully acknowledged for supporting the Network Project (NWP051).

■ REFERENCES

(1) Barthlott, W.; Neinhuis, C. *Planta* **1997**, *202*, 1–8.
(2) Gao, X.; Jiang, L. *Nature* **2004**, *432*, 36–38.
(3) Zhai, L.; Berg, M. C.; Cebeci, F. C.; Kim, Y.; Milwid, J. M.; Rubner, M. F.; Cohen, R. E. *Nano Lett* **2006**, *6*, 1213–1217.
(4) Burton, Z.; Bhushan, B. *J. R. Soc. Interface* **2007**, *4*, 643–648.
(5) Bhushan, B.; Jung, Y. C. *J. Phys.: Condens. Matter* **2008**, *20*, 1–24.
(6) Bhushan, B.; Jung, Y. C. *Nanotechnology* **2006**, *17*, 2758–2772.
(7) Koch, K.; Bhushan, B.; Barthlott, W. *Soft Matter* **2008**, *4*, 1943–1963.
(8) Samuel, J. D. J. S.; Ruther., P.; Frerichs, H.-P.; Lehmann, M.; Paul, A.; Ruhe, J. *Sens. Actuators, B* **2005**, *110*, 218–224.
(9) Zhao, Y.; Cho, S. K. *Lab Chip* **2006**, *6*, 137–144.
(10) Kanagasabapathy, S.; Baumgart; R. J.; Dituro, M. A.; Su, W. C.; Lockwood, F. E. Hydrophobic self-cleaning coating compositions. U.S. Patent 2008/0221009 A1, September 11, 2008.
(11) Kaiser, M.; Foor, B. S. Hydrophobic coating systems, suspensions for forming hydrophobic coatings, and methods for fabricating hydrophobic coatings. U.S. Patent 2009/0181237 A1, July 16, 2009.
(12) Branson, E. D.; Shah, P. B.; Singh, S.; Brinker, C. J. Preparation of hydrophobic coatings. U.S. Patent 7 485 343, February 3, 2009.
(13) Gau, H.; Herminghaus, S.; Lenz, P.; Lipowsky, R. *Science* **1999**, *283*, 46–49.
(14) Liu, T.; Chen, S.; Cheng, S.; Tian, J.; Chang, X.; Yin, Y. *Electrochim. Acta* **2007**, *52*, 3709–3713.
(15) Quere, D. *Rep. Prog. Phys.* **2005**, *68*, 2495–2532.
(16) Satoh, K.; Nakazumi, H. *J. Sol-Gel Sci. Technol.* **2003**, *27*, 327–332.
(17) Kako, T.; Nakajima, A.; Irie, H.; Kato, Z.; Uematsu, K.; Watanabe, T.; Hashimoto, K. *J. Mater. Sci.* **2004**, *39*, 547–555.
(18) Sun, T.; Feng, L.; Gao, X.; Jiang, L. *Acc. Chem. Res.* **2005**, *38*, 644–652.
(19) Song, W.; Lima, A. C.; Mano, J. F. *Soft Matter* **2010**, *6*, 5868–5871.
(20) Marmur, A. *Langmuir* **2003**, *19*, 8343–8348.
(21) Whyman, G.; Edward, B.; Stein, T. *Chem. Phys. Lett.* **2008**, *450*, 355–359.

(22) Ishino, C.; Okumura, K. *Eur. Phys. J.* **2008**, *25*, 415–424.
(23) Cassie, A. B. D; Baxter, S. *Trans. Faraday Soc.* **1944**, *40*, 546–551.
(24) Fang, J.; Wang, H.; Xue, Y.; Wang, X.; Lin, T. *ACS Appl. Mater. Interfaces* **2010**, *2*, 1449–1455.
(25) Liao, S. K.; Wan, A.; Batteas, D. J.; Bergbreiter, E. D. *Langmuir* **2008**, *24*, 4245–4253.
(26) Liu, H.; Szunerits, S.; Pisarek, M.; Xu, W.; Boukherroub, R. *ACS Appl. Mater. Interfaces* **2009**, *1*, 2086–2091.
(27) Artus, G. R. J; Jung, S; Zimmermann, J.; Gautschi, H. P.; Marquardt, K.; Seeger, S. *Adv. Mater.* **2006**, *18*, 2758–2762.
(28) Budunoglu, H.; Yildirim, A.; Guler, M. O.; Bayindir, M. *ACS Appl. Mater. Interfaces* **2011**, *3*, 539–545.
(29) Dorer, C; Ruhe, J. *Soft Matter* **2009**, *5*, 51–61.
(30) Du, X.; Li, X.; He, J. *ACS Appl. Mater. Interfaces* **2010**, *2*, 2365–2372.
(31) Erbil, H. Y.; Demirel, A. L.; Avei, Y.; Mert, O. *Science* **2003**, *299*, 1377–1380.
(32) Han, J. T.; Lee, D. H.; Ryu, C. Y.; Cho, K. *J. Am. Chem. Soc.* **2004**, *126*, 4796–4797.
(33) Yu, X.; Wang, Z.; Jiang, X. *Langmuir* **2006**, *22*, 4483–4486.
(34) Shirtcliffe, N. J.; McHale, G.; Newton, M. I.; Zhang, Y. *ACS Appl. Mater. Interfaces* **2009**, *1*, 1316–1323.
(35) Chevallier, P.; Turgeon, S.; Bournet, C. S.; Turcotte, R.; Laroche, G. *ACS Appl. Mater. Interfaces* **2011**, *3*, 750–758.
(36) Li, Y; Lee, E. J; Cho, S. O. *J. Phys. Chem. C* **2007**, *111*, 14813–14817.
(37) Xu, Yao.; Fan, W. H.; Zhi, H. Li.; Dong, W.; Sun, H. Y. *Appl. Opt.* **2003**, *42*, 108–112.
(38) Prakash, S. S.; Brinker, C. J.; Hurd, A. J. *J. Non-Cryst. Solids* **1995**, *190*, 264–275.
(39) Gurav, B.; Latthe, S. S.; Kappenstein, C.; Mukherjee, S. K.; Rao, V. A.; Vhatkar, S. R. *J. Porous Mater.* **2011**, *18*, 361–367.
(40) Philipavicius, J.; Kazadojev, I.; Beganskiene, A.; Melninkaitis, A.; Sirutkaitis, V.; Kareiva, A. *Mater. Sci.* **2008**, *14*, 283–287.
(41) Prakash, S. S.; Brinker, C. J; Hurd, A. J.; Rao, S. M. *Nature* **1995**, *374*, 439–443.
(42) Barkhudarov, P. M.; Shah, P. B.; Watkins, E. B.; Doshi, D. A.; Brinker, C. J; Majewski, J. *J. Corros. Sci.* **2008**, *50*, 897–902.
(43) Manca, M.; Cannavale, A.; Marco, L. D.; Arico, A. S.; Cingolani, R.; Gigli, G. *Langmuir* **2009**, *25*, 6357–6362.
(44) Rao, A. V.; Latthe, S. S.; Nadargi, D. Y.; Hirashima, H.; Ganesan, V. *J. Colloid Interface Sci.* **2009**, *332*, 484–490.
(45) Iler, R. K. *The Chemistry of Silica*; John Wiley and Sons: New York, 1979; p 693.
(46) Rao, A. P.; Rao, A. V.; Pajonk, G. M. *Appl. Surf. Sci.* **2007**, *253*, 6032–6040.
(47) The quarter wavelength optical design for single layer AR coating at a particular wavelength λ_0 is given by the equation $\lambda_0 = 4n_f d$ (d = physical thickness of the coating; n_f = refractive index of film), i.e., the reflection will be decreased at the wavelength near the quarter wavelength optical thickness. In general the ideal condition to meet the AR property is $(n_f = n_a n_s)^{1/2}$ where n_a and n_s are the refractive indices of the air and the substrate, respectively.
(48) Yabu, H.; Shimomura, M. *Chem. Mater.* **2005**, *17*, 5231–5234.
(49) Xu, Q. F.; Wang, J. N.; Sanderson, K. D. *ACS Nano* **2010**, *4*, 2201–2208.
(50) Zanaveskin, M. L.; Roshchin, B. S.; Grishchenko, Yu. V.; Azarova, V. V.; Asadchikov, V. E.; Tolstikhina, A. L. *Crystallogr. Rep.* **2008**, *53*, 701–707.
(51) Krustev, R; Muller, H. J.; Toca-Herrera, J. L. *Colloid Polym. Sci.* **1998**, *276*, 518–523.
(52) Abbasian, A.; Ghaffarian, S. R.; Mohammadia, N.; Fallahi, D. *Colloids Surf., A* **2004**, *236*, 133–140.
(53) Holdgate, M. W. *J. Exp. Biol.* **1955**, *32*, 591–617.
(54) Wu, S. Y.; Hsueh, H. S.; Huang, M. H. *Chem. Mater.* **2007**, *19*, 5986–5990.
(55) Grilla, A.; Neumayer, D. A. *J. Appl. Phys.* **2003**, *94*, 6697–9707.
(56) Hong, J. K.; Kim, H. R.; Park, H. H. *Thin Solid Films* **1998**, *332*, 449–454.
(57) Ifuku, S.; Tsuji, M.; Morimoto, M.; Saimoto, H.; Yano, H. *Biomacromolecules* **2009**, *10*, 2714–2717.
(58) Both the low and high thickness films were also observed by low-magnification FESEM. In all cases complete coverage of the glass surface by the films was observed.
(59) Su, Y.; Ji, B.; Zhang, K.; Gao, H.; Huang, Y.; Hwang, K. *Langmuir* **2010**, *26*, 4984–4989.
(60) Ressive, A.; Varaka, M. G.; Laurell, T. *Biotechnol Annu Rev.* **2007**, *13*, 149–200.